Time-Varying Electrostatic Modeling Techniques

David M. Hull
U.S. Army Research Laboratory
Adelphi, MD 20783-1197
Phone: 301-394-3140
email: hull@arl.mil

Abstract

ARL developed computer models and modeling techniques based on the Method of Moments, and has used them for some time to study electrostatic fields associated with targets, terrain clutter, and sensors of interest. Recent extensions to these unique ARL capabilities allow some dynamic conditions to be modeled as a time series of quasi-static models. These new techniques have enabled us to study the extremely low-frequency (ELF) effects of rotating helicopter blades on both airborne and remote sensors. Examples show how a dynamic helicopter model can be used to compute time-varying airborne fieldmeter calibration factors for aircraft charge and atmospheric electric field measurements, and remote ELF electric fields which might be detected by passive surveillance sensors.

Introduction

Numerical analysis techniques are widely used today to solve electromagnetic field problems that are too complex to be solved by analytical methods alone. We chose to develop a significant electrostatic modeling and analysis capability based on the *Method of Moments*, as described by Harrington [1]; this approach is sometimes called the *Method of Subsections* [2] or the *Moment Method* [3]. Unlike the more popular finite-element approach, one does not solve for fields directly, but rather for the field *sources* (in our case, the charge distribution). Once the field sources have been determined, the fields can be readily computed as needed, using the *Principle of Superposition* [4].

To compute the field sources, the governing differential equations (in our case, the Laplace or Poisson equations) are transformed into integral identities, which are applied to a finite number of *elements* that form the boundary surfaces of the field problem. A system of linear equations is defined that satisfy the boundary conditions at each element. In general, the coefficient matrix associated with the resulting system of equations is dense, non-symmetric, and not diagonally dominant, so direct linear system solvers must be used. We have successfully developed models with over 5000 elements.

As applied to electrostatic boundary-value problems, this method is summarized as follows. In a region of constant permittivity ε and a volume charge distribution $\rho(x,y,z)$, the electrostatic potential $\phi(x,y,z)$ satisfies the Poisson equation:

$$-\varepsilon\nabla^2\phi(x,y,z)=\rho(x,y,z). \qquad (1)$$

Dirichlet boundary conditions are those conditions for which the scalar potential is specified at every point on the conductor-dielectric boundary. Under these conditions, the unique solution to this problem is:

$$\phi(x',y',z')=\frac{1}{4\pi\varepsilon}\int_x\int_y\int_z\frac{\rho(x,y,z)}{r(x,y,z)}dxdydz, \qquad (2)$$

where r is the distance between the source point (x,y,z) and the field point (x',y',z'):

$$r(x,y,z)=\sqrt{(x-x')^2+(y-y')^2+(z-z')^2}. \qquad (3)$$

In general, we cannot solve equation (2) at every point on the boundary surfaces. However, we can divide the boundaries up into N elements. For each element, we define a linear equation:

$$\frac{1}{4\pi\varepsilon}\sum_{m=1}^{N}a_{nm}\rho_m=V_n \qquad n=1,2,\ldots,N. \qquad (4)$$

In this way, we have reduced our problem to that of solving the matrix equation:

$$\frac{1}{4\pi\varepsilon}A\rho=V. \qquad (5)$$

The coefficient matrix A can be thought of as an "inverse capacitance density" matrix. The coefficients describe the mutual coupling between the elements, and are defined in terms of the size and orientation of each element relative to the others:

$$a_{nm}=\int_m\frac{1}{r(x,y,z)}dm, \qquad (6)$$

where the field point (x',y',z') in the function r is chosen to be the centroid of element n, and the integration is carried out over element m. The potential vector V specifies the Dirichlet boundary conditions over the boundary surfaces. The elements of the solution vector ρ_n are the modeled charge densities for each element.

Generally, we model charged objects as equipotential surfaces. This does not mean that these objects are "good" conductors, only that the charge relaxation time (i.e., the time needed to redistribute any charge to the steady-state conditions) is small, compared to the time associated with any changes in the specified boundary conditions. To be more precise, we should say we are solving *quasi-static* boundary-value problems. Time-varying boundary conditions can be modeled with a time-series of quasi-static models, up to the frequency at which these assumptions are no longer valid. This upper-frequency limit is dependent on the size and conductivity of the objects being modeled, and on the rate of change of the boundary conditions. The series of quasi-static models is called a *dynamic model*; each quasi-static model in a series is called a *frame*.

Dynamic Hind-D Helicopter Model

To construct the first frame, the surface of the Hind-D (shown in figure 1), was divided into small trapezoids (often rectangles). Each of these 1167 areas is represented as a line segment, as shown in figure 2. These elements are normally positioned in the middle of each area, although they can also be placed on the edges to better model the rapid increases in surface charge densities in those areas. Each element is assigned a constant (linear) charge density using the Method of Moments; the modeled surface charge distribution can vary with the inter-element spacing. The dynamic model is constructed with the five-blade main rotor turning at 240 rpm (4 rps), and the three-blade tail rotor turning at 1200 rpm (20 rps). In this way, we constructed a self-looping high-resolution model (with frames every 2° of main rotor travel), using 36 individual quasi-static models.

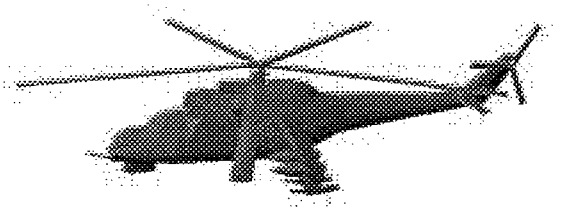

Figure 1. Surface model of Hind-D helicopter.

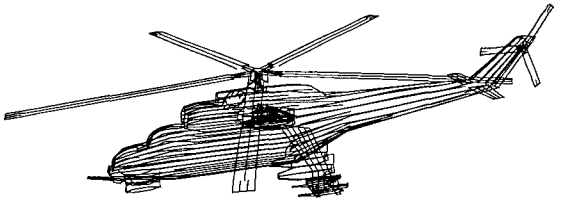

Figure 2. Line-segment model of Hind-D helicopter.

Each frame in the dynamic charge model is the solution to the Laplace equation subject to modified Dirichlet boundary conditions. Specifically, at each time instant, we assumed that the potential was constant over the entire surface of the aircraft; however, we also assumed that this potential "floated" about some mean in such a way that the total aircraft charge remained constant throughout the time series. Since $Q = CV$, the modeled potential varies inversely with the capacitance. Summary information is shown in table 1 for every third quasi-static model; the curves in later figures use data from all 36 frames.

For the Hind-D with a 5-blade main rotor, the capacitance varies by less than 0.5 percent about the mean, as a function of blade phase. Other researchers have reported changes in capacitance of more than ±3 percent for a similar-sized Seahawk helicopter, which has only four main rotor blades [5]. It is reasonable to assume that this effect would be even greater for a UH-1 (Huey) or an AH-1 (Cobra), since these older U.S. helicopters have only two main rotor blades.

Table 1. First-order helicopter charge statistics.

Time (ms)	Rotor (deg) Main	Rotor (deg) Tail	Charge Q (μC)	Cap. C (pF)	Voltage V (V)
0.00	0	0	5.086	510.3	9966
4.17	6	30	5.086	509.9	9973
8.33	12	60	5.086	509.3	9985
12.50	18	90	5.086	509.0	9992
16.67	24	120	5.086	508.2	10007
20.83	30	150	5.086	507.0	10031
25.00	36	180	5.086	506.5	10042
29.17	42	210	5.086	507.0	10030
33.33	48	240	5.086	507.9	10013
37.50	54	270	5.086	508.5	10001
41.67	60	300	5.086	509.1	9989
45.83	66	330	5.086	510.1	9971

It is obvious that the charge *on* the blades must move *with* the blades. Perhaps not so obvious is the fact that, as the blades turn, charge moves on and off the blades in concert with the changing boundary conditions. Indeed, the total available charge is continually redistributed over the entire surface of the aircraft as the main and tail rotors turn. An animated "movie" which shows the movement of charge over time with false color is accessible via the World Wide Web [6].

Figure 3 shows the movement of the electrostatic charge centroid about the mean, as a function of main rotor blade phase in each of the three Cartesian directions. Since there are five main rotor blades, there are five main "beats" in these functions for each complete revolution of the main rotor. As expected, the tail rotor effects are at a frequency three times that of the main rotor, and are most noticeable in the Z (up-down) direction.

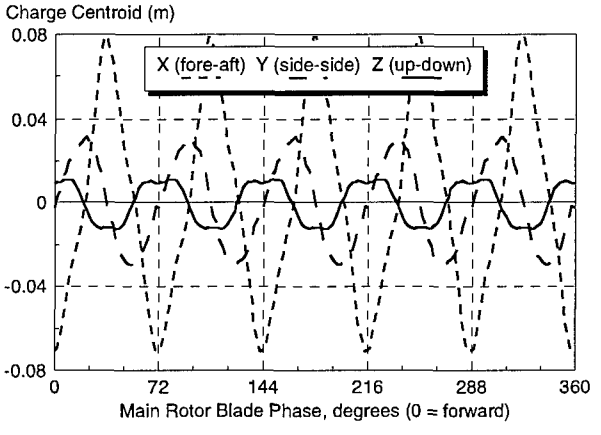

Figure 3. Hind-D charge centroid.

Focus on the Rotor Blades.

Figure 4 shows the percent of total helicopter charge that is present at any given time on two selected rotor blades. The main and tail rotor blades chosen are defined to face forward at zero phase. The other four main rotor blades carry the same charge as the one shown, but staggered in time by 72° increments. Similarly, the charge on the other two tail rotor blades is offset by increments of 24° (or 120° of tail-rotor travel). From the figure, it can be seen that, at any given point in time, over half of the total helicopter charge resides on the blades.

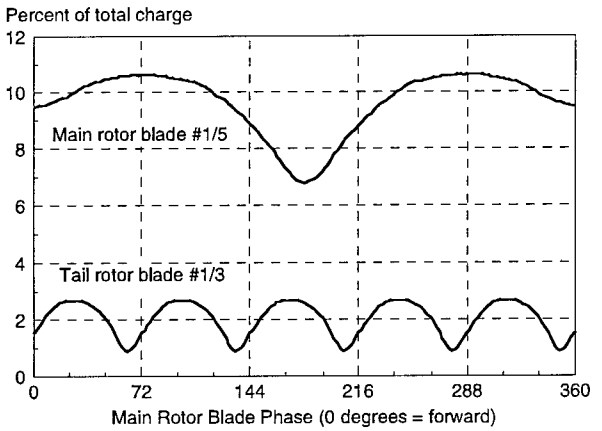

Figure 4. Charge on selected rotor blades.

We can also use the dynamic model to estimate various currents that are flowing over the airframe. These currents are directly proportional to the airframe charge, which we assume to be 5.1 μC. In the case of the main rotor, we have ±2 percent of 5.1 μC (moving on and off each blade) at a fundamental frequency of 8 Hz (there are two minima and two maxima per revolution). If we treat the oscillating charge as a simple sinusoid, and differentiate with respect to time, we expect a peak current flowing between the rotor hub and each blade of about 5 μA. For a more precise estimate, we can numerically differentiate the computed charge functions shown in figure 4 with respect to time. These currents are shown in figure 5.

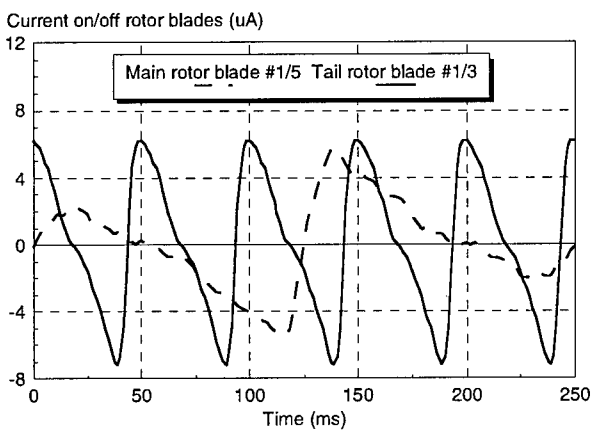

Figure 5. Current at roots of selected rotor blades.

Application of the Model to the Airborne Fieldmeter Calibration Problem

Continuous measurements of aircraft charge and/or atmospheric electric fields (E-fields) can be made during flight operations using one or more *fieldmeters* mounted on the surface of a test aircraft. These instruments use a rotor to alternately shield and unshield stationary sensing elements; this "chopping" technique allows DC (and extremely low-frequency AC) E-fields to be detected. In practical measurement scenarios, the measured electric field at any given point on the aircraft (E_n) is equal to a weighted sum of the aircraft charge (Q) and the ambient atmospheric field (E_x, E_y, E_z):

$$E_n = k_{vn}\frac{Q}{C} + k_{xn}E_x + k_{yn}E_y + k_{zn}E_z, \qquad (7)$$

where the four k terms are called the *field enhancement factors* at each fieldmeter location n. These factors vary as a function of the size and shape of the aircraft, and of the position of the sensor on the aircraft. Since the enhancement factors apply to fixed fieldmeter locations, they are usually considered constants. The calibration problem becomes one of precomputing the enhancement factors. Once these factors are known, the measured fields can be related to the actual quantities of interest: the aircraft charge and/or the ambient electric field.

If four fieldmeters are used, four equations can be solved for the four unknowns (Q, E_x, E_y, and E_z) at any point in time. It has been shown that estimates of aircraft charge and ambient atmospheric fields are sensitive to errors in calibration factors [7]. Moreover, the degree of sensitivity is related to the choice of fieldmeter locations on the surface of the aircraft.

If helicopters are used as the test aircraft, the size and shape of the overall airframe is modulated by the rotor blades, and the enhancement factors can no longer be considered to be constant (in general). For the present discussion, we will limit ourselves to examination of variations in the k_{vn} terms, but we note that similar effects are expected for the other factors.

The amplitudes and phases of the AC components of the enhancement factors are due to the position of the fieldmeters relative to the rotor blades. Computed factors at four selected locations on the fuselage of the Hind-D are shown in figure 6. The model shows that these enhancement factors can vary from less than 1 percent about their mean (as in the "bottom" location) to more than ±20 percent (as in the "top" location).

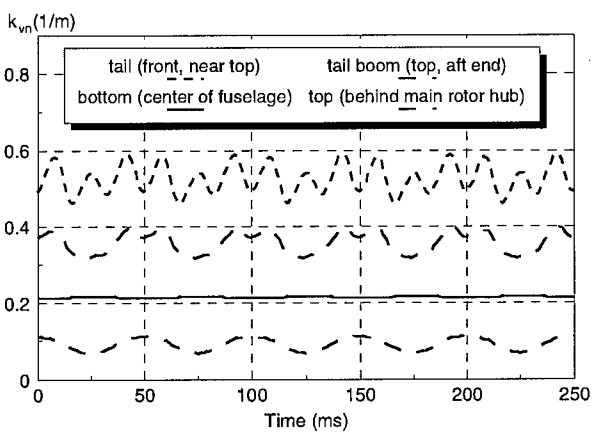

Figure 6. Selected electric field enhancement factors.

The "top" and "bottom" locations on the Hind-D model were chosen to correspond to the fieldmeter positions used in earlier UH-1 charge measurement field tests [8]. In these field experiments, we assumed a constant calibration factor for both locations. The published aircraft potential data shows a pronounced oscillation at the main rotor blade beat frequency for the "top" sensor that is not present in the data for the "bottom" sensor, as we would have predicted using this type of model.

Computation of External ELF E-fields

We defined our model so that the total aircraft charge is constant, with respect to time. We computed the charge centroid as a function of time, and we note from figure 3 that the modulation of the centroid is approximately sinusoidal at the beat frequency of the main rotor. We also note that, for the surveillance scenario, typical aircraft-to-sensor surveillance distances ($r \approx 1$ km) are much larger than the source dimensions ($d \approx 0.1$ m for the centroid or $d \approx 10$ m for the entire aircraft), and are much smaller than the wavelengths of the frequencies of interest ($\lambda \approx 10$ Mm). Therefore, as a first approximation, it makes sense to treat the entire aircraft as an oscillating point source (or *current element*), and to apply the harmonic analysis suggested by Jackson [9] for the near (static) zone (where $d \ll r \ll \lambda$). The dominant E-fields due to the oscillating charge have dipole characteristics; for this reason, the current element is sometimes called a *Hertzian dipole* [10]. In the near zone, the quasi-stationary E-fields are:

$$E_r = \frac{Ql\cos\theta}{2\pi\varepsilon r^3} e^{j\omega(t-\beta)}, \qquad (8)$$

and

$$E_\theta = \frac{Ql\sin\theta}{4\pi\varepsilon r^3} e^{j\omega(t-\beta)}, \qquad (9)$$

where l is the "length" of the Hertzian dipole, θ is the angle between the dipole direction and the field direction, ω is the angular frequency of the oscillation, and β is a phase term. Assuming a total charge Q of 5.1 μC (as in table 1) and a dipole length l of 0.15 m (from figure 3), we estimate the largest field component at a sensor 1 km in front of the helicopter ($r_x = 1000$ m) to be E_x; we expect $E_x(t)$ ($= E_r(t)$ here) to have a peak amplitude of 14 μV/m, and to be in-phase with $Q_x(t)$.

It is interesting to compare the computed "dipole" fields (due to the current, or *movement* of charge in our simplified point-charge model) with the quasi-static fields (due to the changing *position* of the charge in our high-resolution model). Once the quasi-static charge distribution (i.e., the charge on each element) is known at each point in time, the quasi-static E-fields can be computed by summing the contributions from each charged element. Figure 7 shows an example of these computations for a sensor 1 km in front of the helicopter.

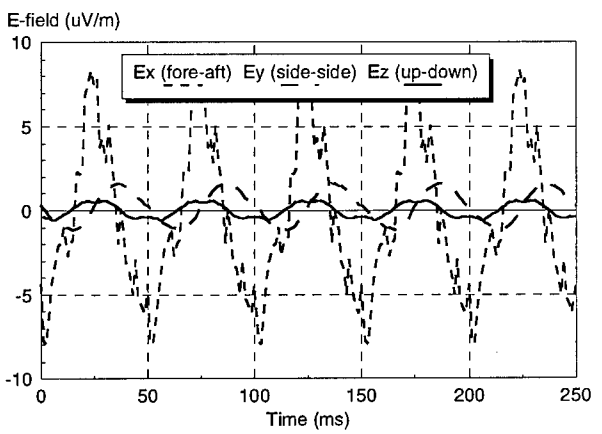

Figure 7. Modeled E-field of Hind-D.

From figure 3, we see that the movement of the charge centroid is *not* sinusoidal. Furthermore, the point-charge model cannot account for any higher-order charge-distribution statistics. Therefore, it may be desirable to develop models that can account for the resulting higher-order current statistics. The model discussed here is a step in that direction.

Conclusions

ARL developed and has used high-resolution quasi-static modeling techniques to investigate electrostatic fields for some time. Recent extensions to these techniques allow the examination of certain ELF fields for sensor applications, both on and off airborne platforms. These fields have radial components and variation with distance that depend on detailed properties of the source. Detailed, dynamic source models allow us to model and investigate these fields at a level not possible with previous techniques.

Acknowledgements

The development of the dynamic Hind-D model, as well as other dynamic models not discussed in this paper, would not have been possible without the exceptional talent and hard work of two undergraduate summer students, Greg Werner and Lisa Zorn. The animated movie on the Web showing the time-varying 3-D charge distribution is a direct result of their efforts, and the underlying models provided a framework for the analysis in this paper.

References

(1) R. Harrington, "Matrix Methods for Field Problems," Proc. IEEE, Vol. 55, No. 2 (Feb 1967), pp 136-149.

(2) D. T. Paris and F. K. Hurd, *Basic Electromagnetic Theory*, McGraw-Hill, New York (1969), pp 181-184.

(3) John D. Kraus, *Electromagnetics*, 4th Edition, McGraw-Hill, New York (1992), pp 81-84.

(4) *Ibid*, pp 52-58.

(5) P. McKenna, R. Dalke, R. Perala, and D. Steffen, "Evaluation of the Observability/Detectability of Electrostatically Charged Rotorcraft," presented at the 1991 Int. Conf. on Lightning and Static Electricity, Cocoa Beach, Florida (April 16-19, 1991). [The paper is not included in the proceedings; more details are included in Electro Magnetic Applications, Inc. Report # EMA-89-R-36, SBIR contract # N00019-88-C-0301 (March 1989).]

(6) http://w3.arl.mil/tto/ARLDTT/FocusTech.html.

(7) K. Hewitt, J. Kositsky, R. Maffione, and J. Thayer, "On the Accuracy of an Aircraft-Borne Ambient Electric-Field Measuring System," presented at the 1989 Int. Conf. on Lightning and Static Electricity, Bath, England, SRI International paper p89-009 (June 1989).

(8) D. Hull and M. Wrenn, "Helicopter Charge Measurements," Harry Diamond Laboratories internal report # R-ST-SA-91-01 (20 Jun 91).

(9) J. D. Jackson, *Classical Electrodynamics*, 2nd Ed., John Wiley & Sons, Inc., New York (1975), pp 391-397.

(10) Paris and Hurd, *op. cit.*, pp 458-463.

INTERNET DOCUMENT INFORMATION FORM

A . Report Title: Time-Varying Electrostatic Modeling Techniques

B. DATE Report Downloaded From the Internet 1/5/99

C. Report's Point of Contact: (Name, Organization, Address, Office Symbol, & Ph #): **U.S Army Research Laboratory**
David M. Hull, (301) 394-3140
Adelphi, MD 20783-1197

D. Currently Applicable Classification Level: Unclassified

E. Distribution Statement A: Approved for Public Release

F. The foregoing information was compiled and provided by:
DTIC-OCA, Initials: VM_ **Preparation Date**: 1/5/99__

The foregoing information should exactly correspond to the Title, Report Number, and the Date on the accompanying report document. If there are mismatches, or other questions, contact the above OCA Representative for resolution.